Materials Reports Solidwaste & Ecomaterials

Materials Reports: Solidwaste and Ecomaterials

Journal Homepage: www.sciopen.com/journal/3078-4093

Original Research Report

Internal strengthening of cement mortar using sustainable functional aggregate with a controlled-release effect

Xiangyu Zhang [1], Shitao Luo [1], Cheng Chen [2], Ahmad Nawaz [1], Leyang Lv [1,*], Yingwu Zhou [1]

[1] Guangdong Provincial Key Laboratory of Durability for Marine Civil Engineering, College of Civil and Transportation Engineering, Shenzhen University, Shenzhen 518000, China

[2] School of Mechanics and Construction Engineering, Jinan University, Guangzhou 510632, China

Abstract: Inspired by the concept of controlled drug release in pharmaceuticals, this study introduces a novel type of functional aggregate designed to enhance the durability of cementitious materials through the controlled release of internal strengthening agents. The effects of functional aggregate incorporation on the fresh and hardened properties, as well as on the durability-related performance of cement mortar, were systematically investigated. The results demonstrated that the prepared functional aggregates exhibited excellent compatibility with the cementitious matrix. Notably, the incorporation of functional aggregates led to a 36.8% reduction in the chloride ion diffusion coefficient and a 6% decrease in water absorption, confirming their effectiveness in improving the durability of cementitious materials. Microstructural analyses revealed that the delayed release of sodium silicate promoted secondary reactions with portlandite, resulting in the formation of a dense alkali calcium silicate hydrate (C-S-H) gel surrounding the functional aggregates. This densified interfacial region significantly enhanced the impermeability and overall durability of the cementitious matrix. The findings of this study provide new insights into the design and fabrication of engineered aggregates with tunable performance, highlighting the potential of using sustainable recycled materials to develop high-durability concrete systems.

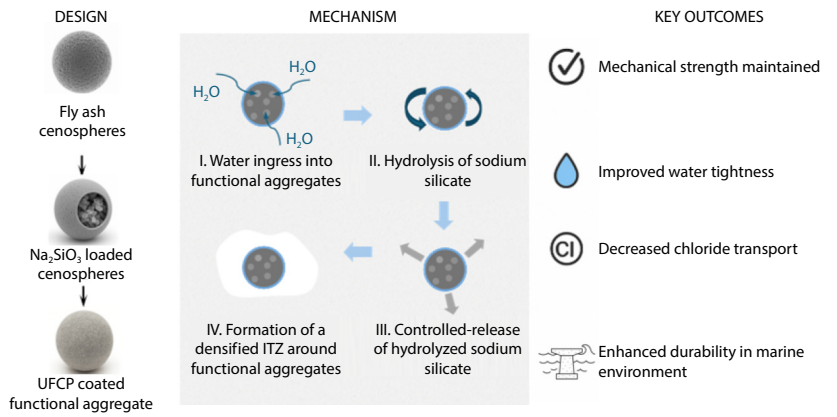

Keywords: functional aggregate, controlled release, chloride resistance, water absorption, alkali calcium silicate hydrate, durability

Citation: X. Zhang, S. Luo, C. Chen, A. Nawaz, L. Lv, Y. Zhou. Internal strengthening of cement mortar using sustainable functional aggregate with a controlled-release effect. *Materials Reports: Solidwaste and Ecomaterials*, 2025, 1: 9520020. https://doi.org/10.26599/MRSE.2025.9520020.

1. Introduction

Concrete durability remains a major challenge in civil engineering, primarily due to the inevitable presence of pores and microcracks in the cementitious matrix, which facilitate the ingress of water and aggressive ions[1]. The penetration of these deleterious ions can induce reinforcement corrosion and alter cement hydration products, ultimately compromising the structural integrity and long-term performance of concrete structures[2,3]. Addressing these durability issues is essential for extending the service life of concrete infrastructure, minimizing maintenance costs, and promoting sustainable development in the construction industry[4,5].

*Correspondence to L. Lv, l.lv@szu.edu.cn

Received 20 June 2025; Received in revised form 13 November 2025; Accepted 3 December 2025

To date, two principal technological approaches have been adopted to enhance the durability of concrete structures: surface coatings[6-8] and internal admixtures[9-12]. Surface coatings are one of the most widely used strategies, as they provide an external protective layer that limits the permeation of water and aggressive ions such as chlorides. Organic coatings, including epoxy resins[13], acrylics[14], or polyurethanes[15], act as physical barriers that inhibit moisture and chemical ingress into the concrete matrix. However, their long-term performance can be compromised by mechanical damage[16], UV degradation[17], and potential delamination over time[18]. Hydrophobic impregnation agents such as silane and siloxane[19-21] can also reduce water penetration by forming water-repellent capillary surfaces; nevertheless, their long-term durability under harsh environmental conditions remains uncertain. Inorganic coatings, such as sodium silicate[22] and cementitious capillary crystalline waterproofing materials (CCCW)[23,24], can chemically react with the cementitious substrate to generate crystalline products within the pores and capillary networks, thereby enhancing the overall impermeability and durability of concrete. However, the penetration depth of such coatings is generally limited, typically ranging from a fraction of a millimeter to several millimeters, depending on the porosity and density of the concrete. Moreover, the effectiveness of surface coatings depends strongly on proper application and maintenance, which may increase costs due to labor-intensive implementation procedures.

Internal admixtures offer an alternative approach to enhancing concrete durability by being incorporated directly during the batching process. These admixtures can interact either physically with the cement matrix as inert fillers[25,26] or chemically with cement hydration products to refine the microstructure of concrete[10,27,28]. Inorganic admixtures, such as silicate-based agents or cementitious capillary crystalline waterproofing (CCCW) materials[23,24], typically react with calcium hydroxide during the early stages of hydration to form additional reaction products. Once incorporated, these admixtures can reduce the permeability of concrete by sealing microcracks, pores, and capillaries, thereby improving resistance to water penetration and mitigating deterioration even under high hydrostatic pressure. In contrast, organic admixtures such as amine- and carboxylic acid-based agents[29,30] are commonly employed as corrosion inhibitors to protect reinforcing steel from chloride-induced corrosion. When reinforced concrete is exposed to a chloride-rich environment, these organic molecules adsorb onto the steel surface, forming a protective film that hinders further corrosion. However, internal admixtures can also pose challenges, including adverse interactions with hydration reactions that may alter setting time[31] or reduce the strength of hardened concrete[30,32].

To mitigate the negative effects of directly mixed internal admixtures on both fresh and hardened concrete properties, a promising strategy involves internal strengthening through the use of encapsulated admixtures that enable targeted release of active components when needed[33-35]. The concept of targeted or controlled release, initially developed in the pharmaceutical industry for site-specific drug delivery[36], has recently been adapted for civil engineering applications to improve the durability of cementitious materials. Kamat et al. developed a novel aggregate-like capsule, namely chitosan–calcium alginate (Cs–CA) capsules, capable of controlled release of sodium ferrocyanide (NaFeCN) within hydraulic mortars to prevent salt weathering over extended periods[37,38]. Although a sustained release of the anti-weathering agent was achieved in lime-based mortars, the compatibility of these capsules with other agents (e.g., silicate-based admixtures) in Portland cement systems remains unclear. Similarly, Li et al. investigated the performance of encapsulated corrosion inhibitors in lightweight concrete[39]. Through the controlled release of sodium monofluorophosphate (Na-MFP) and its subsequent reaction with Ca^{2+} ions, a protective $Ca_3(PO_4)_2$ layer formed on the reinforcing steel surface, enhancing corrosion resistance. Nevertheless, the inclusion of lightweight aggregates (LWAs) can adversely affect the compressive strength of concrete, unless they are subjected to special treatment[40,41]. Therefore, further research is required to develop engineered aggregates capable of controlled release of functional admixtures without compromising the mechanical performance of the host matrix.

Fly ash cenospheres (FACs) are unique by-products of coal combustion, typically produced in thermal power plants[42,43]. These hollow, lightweight particles exhibit bulk densities ranging from 200 to 1000 kg m^{-3} and average diameters between 20 and 600 μm. Owing to their low density, high strength, and excellent thermal insulation properties, FACs have been widely utilized in cementitious systems for density reduction[44], improved thermal insulation[45], and enhanced resistance to fire and freeze–thaw cycles[46]. Recent developments have demonstrated the potential of modified FACs as aggregate-like containers for the functional design of cementitious materials. For example, Liu et al.[47] fabricated an internal curing agent by etching FACs with hydrofluoric acid, followed by encapsulation of water. Mortar specimens containing up to 9% (by cement weight) of this internal curing agent exhibited total shrinkage rates below 20 με after 7 d, attributed to the gradual release of stored water from the perforated cenospheres during hydration.

Building upon this concept, the present study explores the feasibility of preparing functional aggregates with delayed-release capability using FACs. By gradually releasing concrete-strengthening agents into the surrounding matrix, these aggregates are designed to mitigate the adverse effects associated with direct admixture blending while simultaneously enhancing the durability of cementitious materials through improved cement hydration. This was achieved by impregnating perforated FACs with sodium silicate, followed by a tailored coating with ultrafine cement powder (UFCP) to form encapsulated functional aggregates. The modified aggregates were then partially substituted for natural aggregates in cement mortar mixtures. The influence of the functional aggregates on both fresh and hardened properties, as well as the effects of delayed silicate release on durability-related performance, was systematically investigated. Furthermore, microstructural analyses, including X-ray diffraction (XRD) and micro-area X-ray fluorescence (XRF) mapping, were conducted to elucidate the working mechanism of the func-

tional aggregates within the cement matrix. This study is anticipated to contribute valuable insights into the rational design and fabrication of engineered aggregates with customizable properties derived from sustainable recycled resources.

2. Materials and methods

2.1. Materials

Sodium silicate (SS, Mw=122 g mol^{-1}) was used as the internal strengthening agent and was obtained from Shanghai Macklin Co., Ltd. Fly ash cenospheres (FACs) with particle sizes ranging from 800 to 1700 μm were employed to prepare the functional aggregates (sourced from Haoda Building Materials Co., Ltd.). The chemical composition of the FACs, determined by X-ray fluorescence (XRF) analysis, is presented in Table 1. To introduce sodium silicate into the FAC shells, the glassy outer layer of the cenospheres was etched using hydrofluoric acid (HF, 1.2 mol L^{-1})[47,48]. Ultrafine cement powder (UFCP; Kangjing Building Materials Co., Ltd.) was then used to regulate the release rate of the internal strengthening agent by sealing the perforations in the FACs.

Commercial ordinary Portland cement (OPC, CEM I 42.5 N) and CEN Standard sand, in accordance with EN 196-1[49], were used to prepare the mortar specimens. The chemical compositions of OPC and UFCP are listed in Table 2, and the particle size distribution of UFCP is shown in Fig. 1. Tap water was used as the mixing water throughout the experiments.

2.2. Preparation of functional aggregates

The functional aggregates containing an internal strengthening agent were developed through a three-step encapsulation process: (1) perforation of the cenospheres via acid etching, (2) loading of the internal strengthening agent, and (3) coating of the loaded FACs with varying dosages of ultrafine cement powder (UFCP). The detailed procedures are described below.

2.2.1. Acid etching

As-received FACs were first dried in a vacuum oven at 200 °C for 24 h. The dried cenospheres were then immersed in a hydrofluoric acid (HF) solution (1.2 mol L^{-1}) and continuously stirred using an agitation impeller for 120 min. To ensure sufficient exposure, 1 L of HF solution was used per 500 g of FACs. After etching, the FACs were filtered using sieves, thoroughly washed with demineralized water to remove residual acid, and dried at 110 °C for 24 h.

2.2.2. Internal strengthening agent loading

Sodium silicate (SS) was loaded into the perforated FACs using a vacuum impregnation method. The FACs were first placed in a vacuum chamber at −0.1 MPa for 1 h to evacuate air from the pores. SS solution, with a volume three times that of the FACs, was then introduced into the chamber until the FACs were fully immersed. Impregnation was maintained under −0.1 MPa for 0.5 h. Subsequently, the SS-loaded FACs were filtered, rinsed with demineralized water, and dried in a rotary dryer for 3 h at 60 °C under hot air, with a rotation speed of 60 r min^{-1}.

2.2.3. UFCP coating

To impart delayed-release functionality, the SS-loaded FACs were coated with UFCP. The hydrated UFCP formed a buffer layer that regulates the release of sodium silicate. To study the effect of coating thickness, the weight ratio of UFCP to FACs was set at 0.5, 1, 2, and 2.5. During continuous rotation in a rotary dryer, the SS-loaded FACs were first sprayed with a fine mist of water to wet the surface. The water film facilitated the adsorption and initial hydration of UFCP. UFCP powder was then blown into the rotary dryer to ensure uniform coverage on the FAC surfaces. The adsorbed water induced hydration of the UFCP, resulting in a thin, uniform cementitious coating around each particle.

2.3. Preparation of mortar specimens

Mortar specimens were prepared by partially substituting natural sand with functional aggregates (with and without UFCP coating) at volumetric ratios of 3%, 5%, and 7%. The water-to-cement ratio for all mixes was 0.5. In each case, Portland cement and sand were first dry-mixed in a planetary mixer for 30 s. Water was then added, and the mixture was stirred at low speed for 90 s, followed by high-speed mixing for an additional 90 s. For the reference mortar directly blended with sodium silicate (Ref-SS), the SS solution was incorporated into the mixing water prior to combining with the dry materials. For mortar containing the prepared functional aggregates (sustainable, controlled-release aggregates), the aggregates were added 30 s before the end of mixing to ensure uniform distribution. The fresh mortar was immediately cast into molds and subjected to external vibration for 1 min to remove air voids. After 24 h, the specimens were demolded and cured in a standard curing room at (20 ± 2) °C and 95% relative humidity until the target age. The mix proportions of the eight mortar samples are summarized in Table 3. Aggregate dosages of 3%, 5%, and 7% were selected to balance performance and structural integrity.

2.4. Characterization of functional aggregate

2.4.1. Morphology

The morphology of the functional aggregate at each stage of

Table 1. Chemical composition of the FACs (wt%).

Composition	SiO_2	Al_2O_3	Fe_2O_3	K_2O	Na_2O	MgO	CaO	Others	LOI
Oxide (%)	57.82	29.57	4.71	2.29	1.93	1.34	1.01	1.15	1.10%

Table 2. Chemical composition of Portland cement (wt%).

Materials	CaO	SiO_2	Al_2O_3	Fe_2O_3	SO_3	MgO	Others	LOI
Cement	63.75	21.91	4.82	3.18	3.29	2.40	0.67	0.1%
UFCP	48.11	26.89	11.23	4.11	2.90	4.73	2.03	0.02%

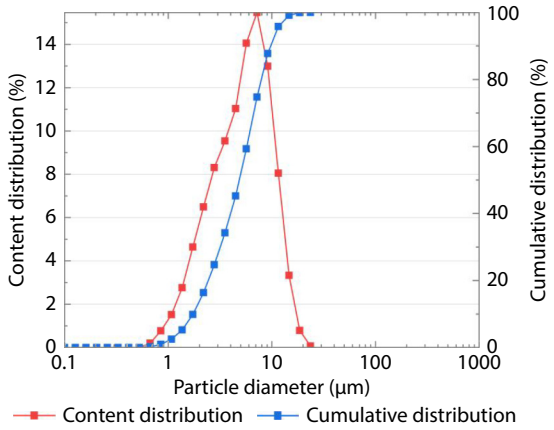

Fig. 1. Particle size distribution of the ultrafine cement powder.

fabrication was obtained using an environmental scanning electron microscope (ESEM, Quanta TM 250 FEG, FEI, United States) at an acceleration voltage of 10 kV. To improve the image resolution, the surface of the specimens was treated with gold coating before the observations. Conductive tape was used to bind the particles on the sample holder.

2.4.2. Release behavior

When SS-loaded functional aggregates were added to water, the sodium silicate dissolved into silicate and sodium ions, resulting in an increase in solution conductivity. To investigate the effect of UFCP coating thickness on the release behavior of the internal strengthening agent, conductivity measurements were performed on the water in which functional aggregates with different coating thicknesses were immersed, using a conductivity meter (DDS-11, Yidian Scientific Instruments Co., Ltd., China). Prior to testing, the electrode was thoroughly rinsed with deionized water. For each measurement, 1 g of functional aggregates (based on the weight of the cenospheres) was added to 50 mL of deionized water. The cleaned electrode was then immersed in the solution, and once the readings stabilized, conductivity values were recorded at regular intervals over a 7-day period, expressed in μS cm^{-1}.

The variation in sodium ion concentration from SS-loaded FACs, with and without UFCP coating, was further quantified using inductively coupled plasma optical emission spectroscopy (ICP-OES, Agilent 5110, Agilent Technologies, USA). Sodium ion leaching reflects the release of sodium silicate from the aggregates into the solution. For the test, the functional aggregates were placed in tea bags and immersed in 50 g of simulated pore solution in glass bottles. Samples were retrieved at 1.5, 3, 6, 12, 24, and 48 h, and the sodium ion concentration in the solution was measured using ICP-OES. The instrument parameters were set as follows: radiofrequency power 1.20 kW, plasma flow rate 12.0 L min^{-1}, auxiliary flow rate 1.00 L min^{-1}, with three replicates for each measurement. The concentration of sodium ions was calculated according to the following equation:

$$Cx(\text{mg kg}^{-1}) = \frac{C_0(\text{mg L}^{-1}) \times f \times V_0(\text{mL}) \times 10^{-3}}{m(\text{g}) \times 10^{-3}} \quad (1)$$

where Cx is the concentration of the substance in mg kg^{-1}; m represents the mass of the sample used for analysis in grams; V_0 denotes the volume of the sample after digestion (mL); C_0 refers to the initial concentration (mg L^{-1}) of the element in the test solution.

2.5. Effect of functional aggregate on mortar

2.5.1. Fresh properties

The effect of the functional aggregate addition on the fresh properties of mortar was studied in terms of workability, setting time, and early shrinkage.

(1) Setting time

The initial and final setting times of cement paste were measured using a fully automatic Vicat apparatus (MATEST E044N, Vicatromic, Italy) following the procedures of European Standard EN 196-3:2005[50]. Readings were recorded at 15-minute intervals until the final set was reached.

(2) Workability

The workability of the mortar mixtures was determined according to ASTM C1437-20[51]. A conical mold with an upper diameter of 70 mm, a lower diameter of 100 mm, and a height of 60 mm was placed at the center of a glass plate. Freshly mixed mortar was poured into the mold and compacted. Excess mortar was removed with a steel trowel, and the mold was then lifted vertically. The mortar was vibrated on a vibrating table at one cycle per second for 25 cycles. After vibration, the diameters of the mortar spread in two perpendicular directions were measured using calipers, and the mean value was taken as the flow diameter.

(3) Early shrinkage

Early-age shrinkage (up to 24 h after mixing) was measured using a shrinkage cone (Schleibinger GmbH, Germany). A plastic reflector plate (20 × 20 mm) was placed on the top surface of the sample, and the displacement of the reflector was continuously monitored using a laser measurement system. The change in distance between the laser emitter

Table 3. Overview of the type of mortar specimens and their mix design.

Label	Cement (g)	Water (g)	Sand (g)	Functional aggregate (g)	SS (g)
Ref	450	225	1350	–	–
Ref-SS	450	225	1350	–	4.5
Noncoat-3%	450	225	1336.5	13.5	–
Noncoat-5%	450	225	1327.5	22.5	–
Noncoat-7%	450	225	1318.5	31.5	–
Coated-3%	450	225	1336.5	27	–
Coated-5%	450	225	1327.5	45	–
Coated-7%	450	225	1318.5	63	–

and the reflector was recorded over 24 h to quantify early shrinkage.

2.5.2. Compressive strength

The effect of functional aggregate incorporation on the mechanical properties of mortar was evaluated by compressive strength testing at 3, 7, and 28 d of curing. Tests were performed using a computer-controlled flexural and compressive testing machine (YAW-300B, Zhejiang Lice Instrument Equipment Co., Ltd., China) at a loading rate of (2400 ± 200) N s^{-1}. For each data point, the compressive strength was obtained as the average of three specimens from each group.

2.6. Durability performance

2.6.1. Porosity

After compressive strength testing, approximately 20 g of crushed mortar fragments was collected to investigate the porosity of the hydrated cement matrix using low-field nuclear magnetic resonance (LF-NMR). The fragments were first immersed in acetone to halt cement hydration and then vacuum-dried at 40 °C. Subsequently, the specimens were saturated with water under vacuum conditions. After saturation, the samples were tightly wrapped in polyethylene film, and their pore structure in the saturated state was analyzed using an LF-NMR system (MesoMR12-060H-I, Suzhou Niumag Analytical Instrument Corp., China). Measurements were conducted using the Carr-Purcell-Meiboom-Gill (CPMG) pulse sequence at 200 kHz, with an echo time (τ) of 100 μs, a repetition delay (TW) of 1500 ms, 2000 echoes (NECH), and 16 accumulations (NS).

2.6.2. Water absorption

Water absorption is an important indicator of the durability of cementitious materials. In this study, it was determined following ASTM C1403-15[52]. Mortar cubes (50 mm) were cast and cured at 95% relative humidity for 28 d. Prior to testing, specimens were oven-dried at (105 ± 5) °C until reaching a constant mass and then stored in a desiccator to prevent moisture uptake before weighing. The initial dry weight (W_1) was recorded, and the specimens were immersed in water at room temperature for 24 h. After immersion, surface water was removed with a damp cloth, and the saturated weight (W_2) was measured. Water absorption was calculated as:

$$Water\ absorption\,(\%) = \frac{W_2 - W_1}{W_1} \times 100\% \quad (2)$$

where W_1 is the dry weight of the specimen, and W_2 is the saturated weight of the specimen.

2.6.3. Chloride diffusion coefficient

The chloride diffusion coefficient of the mortar was evaluated using the rapid chloride migration (RCM) test, following NT Build 492[53]. Cylindrical specimens (100 mm diameter × 50 mm height) were used. The anode electrolyte consisted of a 0.3 M NaOH solution, and the cathode electrolyte was a 10% NaCl solution. A constant voltage of 30 V was applied across each specimen, and the initial current was recorded. After the test, specimens were split along the diagonal, and the depth of chloride penetration was determined by spraying the freshly split surface with a 0.1 M $AgNO_3$ solution. The non-steady-state migration coefficient was calculated using the following formula:

$$D_{RCM} = \frac{0.0239 \times (273 + T)\,L}{(U - 2)\,t}\left(X_d - 0.0238\sqrt{\frac{(273 + T)LX_d}{U - 2}}\right) \quad (3)$$

where D_{RCM} is the non-steady-state migration coefficient ($\times 10^{-12}$ m^2 s^{-1}), T is the average temperature in the anode solution (°C), L is the thickness of the specimen (mm), U is the applied voltage (V), X_d is the average chloride penetration depth (mm), t is the duration of the test (hours).

2.7. Mechanism analysis

2.7.1. Mineral composition

X-ray diffraction (XRD) analysis was performed using a Bruker D8 diffractometer in a θ–2θ configuration with monochromatic Cu Kα radiation, equipped with a LYNXEYE detector. The generator voltage and current were set to 40 kV and 40 mA, respectively. Data were collected over a 2θ range of 5°–70° with a step size of 0.02°. To prevent further hydration reactions, mortar specimens were first crushed, immersed in acetone for 24 h, and then ground into powder using an agate mortar. Excess acetone was removed by vacuum filtration, and the powder was dried in an aerated oven at 60 °C for 24 h. The dried samples were passed through an 80 μm sieve and vacuum-sealed in plastic bags until analysis.

2.7.2. Micro-XRF

To examine the release behavior of the internal strengthening agent from the functional aggregates, micro-X-ray fluorescence (μ-XRF; M4 TORNADO PLUS, Bruker, Germany) was employed to map the elemental distribution around the aggregates within the mortar matrix. The X-ray tube operated at 50 kV and 600 μA under vacuum (2 mbar). The excitation beam had a spot size of approximately 20 μm, and elemental maps were collected with a pixel size of 15 μm. The scan area measured 197 × 205 pixels (2.96 mm × 3.07 mm), with a pixel dwell time of 10 ms per pixel.

3. Results and discussion

3.1. Characterization of functional aggregates

3.1.1. Morphology

Fig. 2 illustrates the morphology of the functional aggregates at different stages of preparation. Compared with the as-received FACs shown in Fig. 2a, the surface of the acid-etched cenospheres in Fig. 2b clearly exhibits perforations. These pores on the outer surface of the perforated cenospheres (P-CS) confirm the successful removal of the glassy-crystalline layer by acid etching, providing channels for the subsequent introduction of sodium silicate solution. Fig. 2c shows the perforated FACs after loading with sodium silicate (SS). The surface pores appear filled, indicating that the SS solution has penetrated and occupied the voids on the FAC surfaces. To further verify the impregnation of SS, the particles were crushed and examined via SEM. The inset image of the cross-section clearly shows that SS was effectively loaded into the internal voids of the hollow microspheres. To

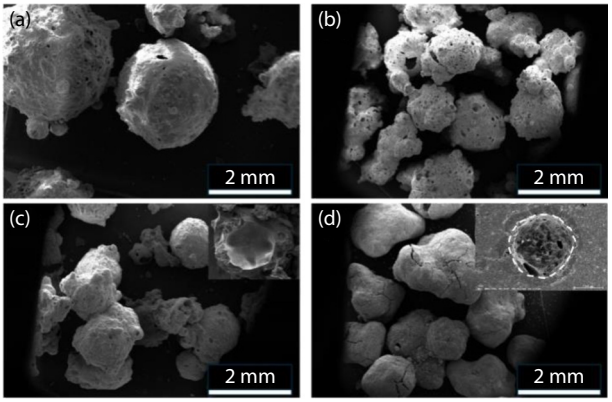

Fig. 2. SEM images showing (a) the as-received FACs, (b) the perforated FACs after acid etching, (c) the SS-loaded FACs, and (d) the final UFCP-coated functional aggregates. The inset in (c) is the cross-section of the SS-loaded FACs.

achieve delayed and controlled release of the internal strengthening agent, the SS-loaded FACs were coated with a penetrable cementitious layer in the final step. Fig. 2d presents the morphology of the fully prepared functional aggregate, showing a uniform coating on the surface. Micro-cracks observed on the coating are likely the result of shrinkage during the hydration of the cementitious layer. The inset in Fig. 2d shows the cross section of the UFCP-coated functional aggregate that was embedded in the cement matrix. The dashed line in white indicates the shell of SS-loaded FACs, while the darker area surrounding the shell indicates the UFCP coating on the SS-loaded FACs, which has been integrated with the cement matrix.

3.1.2. Release behavior

The internal strengthening agent, sodium silicate (SS), is a water-soluble compound that dissociates into sodium and silicate ions upon contact with water. The release behavior of SS from the functional aggregates was evaluated by measuring the conductivity of water solutions containing the aggregates. Fig. 3 presents the conductivity profiles of functional aggregates with different UFCP coating thicknesses. The marked differences in conductivity indicate that the coating effectively controls the release rate of SS. Uncoated functional aggregates (Ref, black curve) exhibit high initial conductivity (above 1500 μS cm^{-1}), which gradually increases over time, indicating rapid leaching of the impregnated SS. In contrast, UFCP-coated functional aggregates show significantly lower initial conductivity. For example, the M0 sample (UFCP-to-FACs ratio of 1:2) exhibits a conductivity of 790 μS cm^{-1} during the first 24 h, increasing to 1700 μS cm^{-1} after 7 d, demonstrating the role of the UFCP coating in regulating SS dissolution. As the UFCP-to-FACs ratio increases from 1:1 (M1) to 2.5:1 (M3), the initial conductivity of M1, M2, and M3 decreases further to approximately 600 μS cm^{-1} or lower. Notably, the conductivity remains nearly constant for the first 24 h before gradually increasing to about 1000 μS cm^{-1}, indicating a delayed release of SS. Previous studies have shown that direct incorporation of SS during mortar mixing can interfere with cement hydration, potentially reducing the overall mechanical and durability performance of cementitious materials[54]. The delayed release of SS from the functional aggregates provides a window for cement hydration, reducing the negative impact of SS on the performance of cementitious materials. Moreover, as the UFCP-to-FACs ratio increases from 1:1 (M1) to 2.5:1 (M3), the initial conductivity shows only minor differences, indicating that increasing the coating thickness beyond a certain point does not significantly alter the release behavior of the functional aggregates.

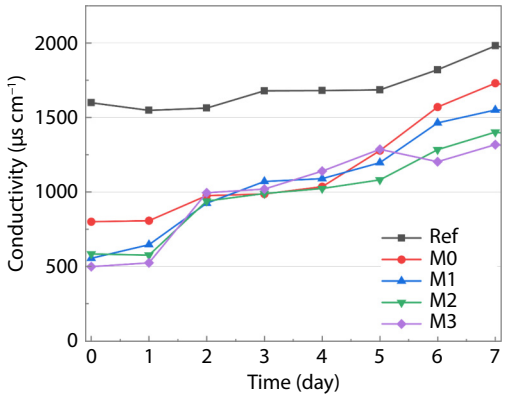

Fig. 3. Conductivity of the solution containing SS-loaded FACs with various UFCP coating thicknesses, where M0, M1, M2, and M3 designate the samples for which the weight ratio of UFCP to FACs was 0.5, 1, 2, and 2.5, respectively, during the coating process.

Fig. 4 presents the ICP test results showing the variation in sodium ion concentration over time after the functional aggregates with and without surface coatings were immersed in water. The red curve represents the ICP result of SS-loaded FACs without UFCP coating, while the blue curve represents the ICP result of the SS-loaded FACs covered with UFCP coating. According to the figure, it can be observed that the SS-loaded FACs without UFCP coating exhibit an immediate increase in sodium ion concentration once they are exposed to water, suggesting a rapid release of sodium silicate from the perforated cenospheres. In contrast, the release rate of sodium ions from the SS-loaded FACs covered with UFCP coating (blue) is significantly slower than that of the SS-loaded FACs without UFCP coating (red), indicating that the coating could effectively reduce the release rate of sodium silicate. The delayed release of sodium silicate was believed to

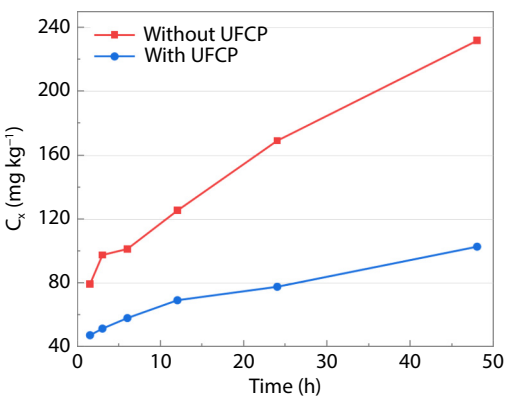

Fig. 4. ICP results showing the variation in sodium ion concentration over time after the functional aggregates with and without surface coatings were immersed in water.

help mitigate the adverse effect of unintentional release of sodium silicate at the cement hydration stage while enhancing the overall durability of the cement matrix by filling voids and micro-cracks surrounding the aggregates.

3.2. Effect of the functional aggregate on the properties of mortar

3.2.1. Fresh properties

The effect of the functional aggregate addition on the fresh properties of mortar was studied in terms of workability, setting time, and early shrinkage. The results are summarized in Table 4. Generally, mortar specimens incorporated with functional aggregate show higher workability than the pure mortar (Ref) or mortar directly mixed with SS (Ref-SS). Past studies have shown that FACs can reduce the surface area to volume ratio, increasing workability even at low *w*/*b* ratios[55]. This differs from the hydrophilic polymer-based capsules, such as chitosan or alginate, which reduced the workability significantly. Moreover, it was found that the workability of Coated-7% specimens is lower than that of Noncoat-7%. This can be attributed to the absorption of water due to the existence of the UFCP coating on the functional aggregates.

As for the setting time, the measured value of Ref-SS specimens is lower than that of Ref, showing that the direct addition of SS accelerates the hydration process of cement paste. This is in good accordance with previous studies[56,57]. In contrast, when the functional aggregate was blended in the mixture, the initial setting time of mortar specimens (Noncoat-7% and Coated-7%) was slightly retarded from 3.8 h to 4.4 h and 4.5 h, respectively. Particularly, the final setting time of the Coated-7% specimen was found to be postponed to 10 h, possibly due to the controlled release effect of the UFCP coating.

The early shrinkage of the freshly blended mixture was monitored using a Shrinkage-Cone, and the results are shown in Table 4. Among the specimens, the Ref-SS specimen shows the minimum volume of shrinkage over this period. The reduced early shrinkage can be attributed to the formation of a gel-like layer when mixed with water, which can reduce the evaporation of water from the cement surface[58]. Conversely, when functional aggregates were mixed in, mortar specimens (Noncoat-7% and Coated-7%) showed a higher volume of shrinkage than the Ref. This is expected and is due to the significantly higher water absorption of functional aggregates compared to that of natural sand. In comparison, Noncoat-7% specimens containing uncoated functional aggregate showed a significantly higher value of early shrinkage than the Coated-7% specimens. This suggests that coating the functional aggregate with UFCP could mitigate the shrinkage of the specimens by regulating the leaching of SS to the surrounding and the absorption of water in the reverse direction.

3.2.2. Compressive strength

Fig. 5 illustrates the impact of functional aggregates addition with different volume ratios (with and without UFCP coating) on the compressive strength of mortar specimens at 3, 7, and 28 d of curing. The figure shows that the pure mortar specimen (Ref) exhibits the highest compressive strength, peaking above 48 MPa at 28 d. The direct addition of sodium silicate (Ref-SS) in mortar results in a progressive reduction in the compressive strength compared to the other specimens. This reduction can be attributed to the dissolution of sodium silicate in water, followed by the immediate reaction between the dissolved silicate and the portlandite, leading to the formation of alkali sodium-calcium-silicate hydrate (NCSH) gel. The formation of an alkaline gel upon introducing sodium silicate into the cement paste contributes to a decrease in the mortar's mechanical strength[54]. In the meantime, it was found that the compressive strength of specimens containing uncoated functional aggregates decreases as the replacement ratio of functional aggregate increases, with Noncoat-7% exhibiting the lowest values. This can be attributed to the release of SS from the cenosphere interrupting the progress of cement hydration and affecting the development of compressive strength. In contrast, specimens containing the UFCP-coated functional aggregates exhibited much better performance in compressive strength. This indicates that the UFCP coating effectively controlled the release of sodium silicate from the FACs at the early age of cement hydration, thereby mitigating the negative impact of the early introduction of sodium silicate on the compressive strength of mortar. Overall, the addition of functional aggregates showed a less adverse effect compared to that reported in the previous study where polymeric capsules were used as self-healing functional additives, resulting in only a 14.5% decrease in compressive strength at a maximal 9% microcapsule content[59].

3.3. Assessment of durability-related performance

3.3.1. Porosity

Fig. 6 illustrates the total porosity (%) of various mortar specimens after 3, 7, and 28 d of curing. A correlation was found between the porosity and the compressive strength of the mortar presented in Fig. 5, indicating that specimens with lower compressive strength typically have higher porosity. For the specimens incorporated with uncoated functional aggregate, porosity was found to increase with a higher percentage of functional aggregate addition, and the Uncoated-7% specimens showed the highest porosity among all mixtures. The higher porosity is believed to originate from the

Table 4. Overview of the measured fresh properties for different mix designs.

Measured properties	Ref	Ref-SS	Noncoat-7%	Coated-7%	Comment
Workability (mm)	173±5	170±4	220±4.5	189±5.3	
Setting time (h)	3.8	2.4	4.4	4.5	Initial
	7	6	7	10	Final
Early shrinkage (μm m^{-1})	−3143	−1800	−4978	−3685	24 h

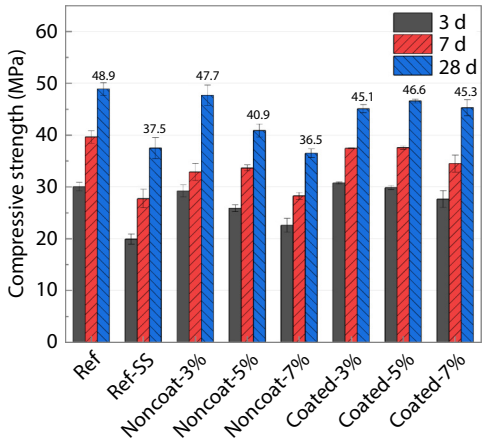

Fig. 5. Compressive strength of mortar specimens at 3, 7, and 28 d with different mix designs.

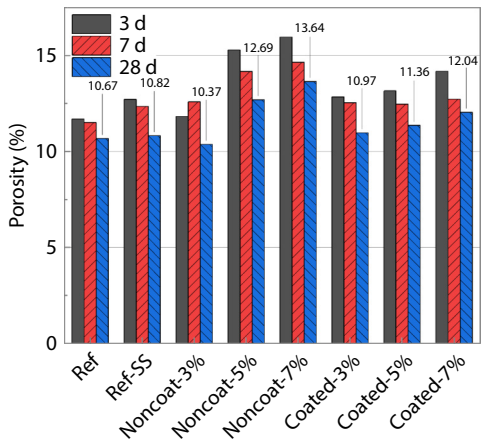

Fig. 6. Total porosity (%) of various cement mortar specimens at 3, 7, and 28 d of curing.

inclusion of more functional aggregates, as the cenospheres used as templates in producing the functional aggregates became pores soon after the release of SS to the cement matrix. In contrast, the specimens containing UFCP-coated functional aggregates (Coated-*x*%) exhibited lower porosity, compared to their counterparts without UFCP coating, especially for the Coated-5% and Coated-7% specimens. Given that the cenosphere templates are intrinsically hollow particles, the reduced porosity indicates that the density of the cement matrix has been accordingly enhanced. This result also suggests that the UFCP coating applied on the surface of the functional aggregates can effectively balance the strength and porosity of the mortar specimens by controlling the release rate of sodium silicate. In addition, it was found that the direct addition of sodium silicate to the mixture (Ref-SS) has a limited effect on the porosity of the specimens. This differs from the compressive strength results in Fig. 5, where Ref-SS specimens showed the lowest value. This can be attributed to the addition of SS, which accelerated the hydration of cement with the formation of hydration products such as NCSH gel, a material believed to have lower mechanical strength than the CSH gel[54].

3.3.2. Water absorption

Fig. 7 presents the water absorption rates of various mortar specimens after 28 d of standard curing. The results show that the mortar directly mixed with sodium silicate solution had the highest water absorption rate (7.1%). Combined with the compressive strength results, this suggests that the direct addition of SS decreases the mortar's density, leading to reduced durability and mechanical strength. In contrast, the samples containing functional aggregates exhibited a slight decrease in water absorption. Specifically, for the samples containing uncoated functional aggregates, the water absorption rates decreased by 2.20% (Noncoat-3%), 3.08% (Noncoat-5%), and 4.46% (Noncoat-7%) compared with Ref, respectively, with the increase in the replacement ratio of functional microspheres from 3% to 7%. This is significantly higher than that reported in a previous study in which saturated lightweight aggregate (SLWA) was employed to reduce the water absorption of mortar specimens[60]. The possible reason is the release of sodium silicate from the functional aggregate that penetrates the surrounding cement matrix, leading to the formation of a diffusion layer of alkaline gel in the surrounding matrix. The formation of this alkaline gel significantly reduces the water absorption of the mortar. When functional aggregates coated with UFCP were incorporated, the water absorption of the mortar further decreased, demonstrating the effectiveness of UFCP coating in further improving the water absorption rate of mortar.

3.3.3. Chloride diffusion coefficient

The chloride diffusion behavior of mortar specimens was assessed by determining the chloride ion diffusion coefficient using the rapid chloride migration (RCM) method. Fig. 8 presents the chloride ion diffusion coefficients of various mortar compositions, and the specific test conditions and values used in the calculation are detailed in Table 5. The chloride ion migration coefficient for mortar mixed directly with sodium silicate (Ref-SS) is 2.17% higher than that of pure OPC mortar (Ref). This implies that the addition of sodium silicate does not mitigate chloride ion penetration but instead may promote it. This is because the direct addition of sodium silicate at the mixing stage delayed the hydration of aluminate in the cement paste with the formation of alkaline gel, which reduced the absorbing capacity of the cement matrix to the

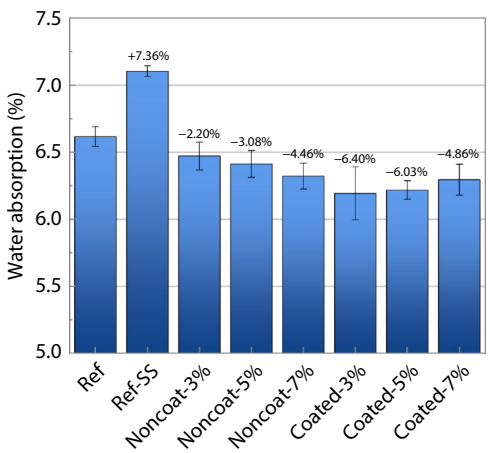

Fig. 7. Water absorption rates of various mortar specimens after 28 d of standard curing.

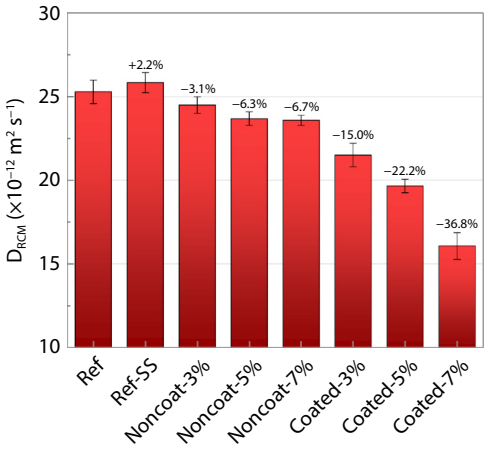

Fig. 8. Chloride diffusion coefficient of various mortar specimens after 28 d of standard curing.

chloride ions[57]. For mortar samples containing uncoated functional aggregates, a reduction in chloride ion migration coefficients was observed as the functional aggregate substitution ratio increased from 3% to 7%. Notably, mortar specimens containing functional aggregates coated with UFCP demonstrated a more significant reduction in chloride ion diffusion. Specifically, the diffusion coefficient for mortar with 3%, 5%, and 7% UFCP-coated functional aggregates decreased progressively by 15%, 22.2%, and 36.8%, compared to the pure OPC mortar. These results confirm that the incorporation of functional aggregates is effective in impeding chloride ion diffusion in mortar specimens. The decrease rate of the chloride ion diffusion coefficient is consistent with that in a previous report in which LDH was employed, specifically where novel zeolite@LDHs core-shell material was employed as a chloride penetration depth reducer[61].

3.4. Microstructural analysis

3.4.1. XRD

To elucidate the mechanism behind the strengthening effect of the proposed functional aggregate with delay-release effect in the cement matrix, a comparison of mineral phases between pure OPC and OPC containing UFCP-coated functional aggregates at 3, 7, and 28 d was made using XRD, and the results are shown in Fig. 9. According to the XRD patterns[62,63], the predominant mineral phases in the two specimens are quartz (Q), calcium silicate (CS, C_3S-C_2S), calcium silicate hydrate (CSH), ettringite (E), and portlandite (P). The primary difference lies in the diffraction intensities of these mineral phases. In the ordinary OPC paste samples (Fig. 9a), the characteristic peak intensity of the portlandite gradually increases as the hydration progresses. This indicates that during hydration, tricalcium silicate (C_3S) and dicalcium silicate (C_2S) react with water with the steady formation of hydration products such as C-S-H gel and portlandite.

In contrast, for the OPC containing coated functional aggregates (Fig. 9b), the peak intensity of portlandite shows a gradual decline from 3 to 28 d, while the peak of CSH becomes more prominent. The primary reason for this phenomenon is believed to be the gradual release of sodium silicate from the FACs, which reacts with portlandite in the surrounding cement matrix, resulting in the formation of alkaline CSH gel in the capillary pores and a reduction in the

Table 5. Specific test conditions and chloride diffusion coefficient.

	U (V)	T (°C)	L (mm)	Depth (mm)	T (h)	D_{RCM} (10^{-12} m^2 s^{-1})
Ref	30	28.445	50.5	49.2	24	25.296
Ref-SS	30	28.875	50.6	49.7	24	25.845
Noncoat-3%	30	28.45	49.6	47.3	24	24.500
Noncoat-5%	30	28.29	49.8	45.6	24	23.690
Noncoat-7%	30	28.31	51.9	43.6	24	23.594
Coated-3%	30	28.24	52.2	39.6	24	21.516
Coated-5%	30	29.26	51	37.0	24	19.667
Coated-7%	30	29.09	49.3	31.4	24	16.078

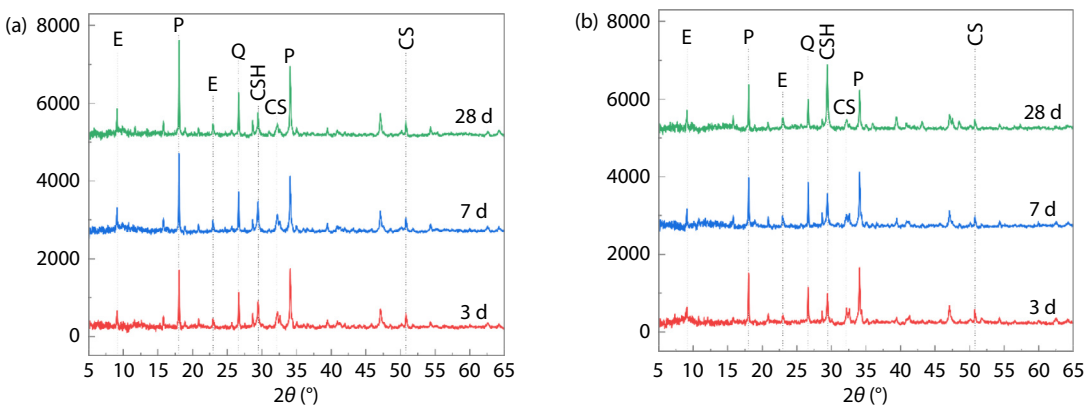

Fig. 9. XRD pattern of (a) OPC and (b) OPC blended with 7% of coated functional aggregate after 3, 7, and 28 d of hydration. The annotations indicate the following: E-ettringite, P-portlandite, Q-quartz, CSH-calcium silicate hydrate, and CS-C_3S/C_2S.

water absorption. The alkaline gel could also serve as a medium for the chloride ion absorption[64]. Interestingly, the timing of this process aligns with the release behavior of functional aggregates in solution, as shown in Fig. 3, thereby verifying the mechanism proposed above by which the functional aggregates enhance the durability of the mortar.

3.4.2. Micro-XRF

To visualize the diffusion of sodium silicate (SS) and the formation of calcium silicate hydrate (CSH) gel around the functional aggregates, the element distribution of ordinary Portland cement (OPC) containing these aggregates was analyzed using micro-area X-ray fluorescence (XRF). Fig. 10 presents the results of this mapping analysis, highlighting the elemental distributions of silicon (Si), aluminum (Al), and sodium (Na), with a focus on the functional aggregate and its surrounding region. In these images, the color scale from red to green to blue represents high, medium, and low element concentrations across the scanning area, respectively. Since the FACs containing SS are primarily composed of SiO_2 and Al_2O_3, the XRF map of aluminum shown in Fig. 10b can be considered as the actual size of the functional aggregates within the cement matrix. Above the shell of FACs, a silicon-rich zone approximately 200–300 μm thick can be observed in Fig. 10c, surrounding the aggregate surface, indicating SS diffusion from the aggregates into the cement matrix. Additionally, the presence of several silicon-enriched areas scattered throughout the image suggests that sodium silicate released from the aggregates has diffused to distant regions and possibly reacted with calcium hydroxide in the cement's pores, with the formation of C-S-H gel. The formation of this additional C-S-H gel is critical for enhancing the water and chloride resistance of cement-based materials. The sodium distribution map in Fig. 10d further confirms this diffusion behavior of SS, as it has a similar pattern of distribution as the silicon element. The reaction between SS and CH was believed to have occurred in these sodium-rich regions.

3.4.3. Detailed mechanism of strengthening mortar using coated functional aggregates

Fig. 11 depicts the schematic diagram of the internal strengthening process in four distinct stages involving the use of coated functional aggregate in mortar. The detailed explanation of each stage is as follows:

Stage I: Initial stage of cement hydration

Environmental water infiltration: At the beginning of the hydration process, external or environmental water penetrates the surface of the coated cenospheres. The hollow structure of the cenospheres allows them to act as reservoirs, absorbing water. This initial absorption of water is crucial for enabling the subsequent internal curing process, as it provides a source of moisture that can be released over time.

Stage II: Acceleration stage of hydration

Sodium silicate hydrolysis: As hydration progresses and enters the acceleration phase, sodium silicate, which is encapsulated inside the coated cenospheres, starts to undergo hydrolysis and breaks down into sodium and silicate ions. This process is slow and controlled, and the hydrolysis reaction helps in gradually releasing water, which aids the ongoing cement hydration.

Stage III: Deceleration stage of hydration

Sodium silicate release: During this stage, hydration slows down (the deceleration phase), and sodium silicate inside the coated cenospheres is continuously released into the surrounding cement paste. The gradual release of dissolved sodium and silicate ions ensures a consistent and prolonged source of water for hydration and formation of alkaline CSH gel by reacting with portlandite.

Stage IV: Stabilization stage of hydration

Solidified region formation: In the final stage, as hydration nears completion and stabilizes, the SS released from the cenospheres fully reacts with portlandite, leading to the formation of a solid, well-structured, alkaline CSH gel around the cenospheres. This solidified region enhances the overall durability of the matrix by filling voids and surface adsorption of harmful ions.

4. Conclusion

In this study, a novel functional aggregate with delayed-release capability was developed by coating sodium silicate—impregnated fly ash cenospheres (FACs) with ultrafine cement powder (UFCP). By enabling the gradual release of sodium silicate, the functional aggregates strengthen the interfacial transition zone and improve overall matrix densification without negatively affecting workability or strength. The incorporation of UFCP-coated functional aggregates significantly reduced up to 36.8% of chloride ion diffusion and 6% of water absorption, demonstrating improved impermeability and durability of cementitious materials. The delayed release of sodium silicate promoted secondary reactions with portlandite, forming dense C-S-H gel around the aggregates, which refined the pore structure and blocked pathways for

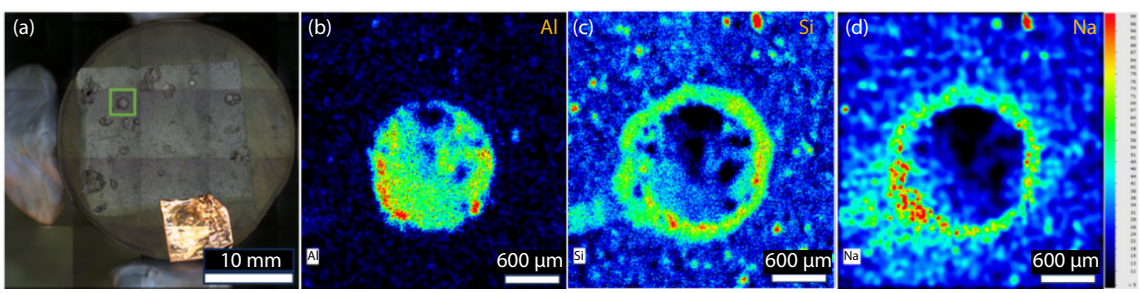

Fig. 10. Images showing (a) the selected location in the micro-region XRF test and the elemental distributions of (b) aluminum element, (c) silicon element, and (d) sodium element.

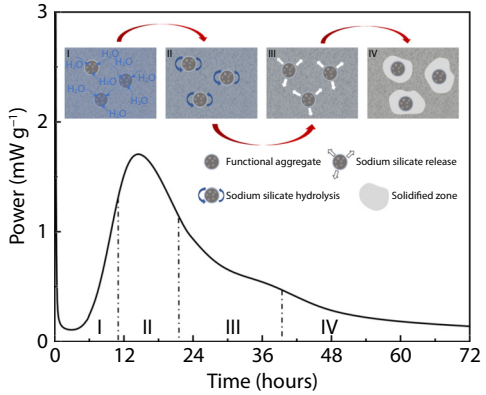

Fig. 11. The four stages of internal curing are as follows: I. During the initial stage of cement hydration, environmental water infiltrates into the cenospheres; II. During the acceleration stage of hydration, sodium silicate within the cenospheres slowly undergoes hydrolysis; III. During the deceleration stage of hydration, sodium silicate inside the cenospheres is gradually released outward; IV. At the stabilization stage of hydration, a solidified region forms around the cenospheres.

water and ion ingress. This self-regulating release mechanism minimizes the maintenance demand for reinforced concrete structures, making it especially suitable for marine environments, underground facilities, and infrastructure exposed to chloride-rich or humid conditions. Furthermore, the use of waste-derived cenospheres aligns with sustainable construction goals, supporting low-carbon and circular economy strategies in the concrete industry.

In future work, research should focus on optimizing coating thickness and release rate to achieve tunable functionality, exploring compatibility with other functional agents (e.g., corrosion inhibitors or self-healing compounds), and conducting field-scale durability evaluations. Such developments could pave the way for the engineering application of controlled-release functional aggregates in high-performance, sustainable concrete infrastructure.

Author contribution statement

Xiangyu Zhang: Investigation. **Shitao Luo:** Formal analysis, Validation. **Cheng Chen:** Validation. **Ahmad Nawaz:** Writing – review & editing. **Leyang Lv:** Conceptualization, Methodology. **Yingwu Zhou:** Supervision, Funding acquisition. All the authors have approved the final manuscript.

Declaration of competing interest

The authors declare that they have no known competing financial interests or personal relationships that could have appeared to influence the work reported in this paper.

Acknowledge

The authors appreciate the financial support from the National Natural Science Foundation of China (No. 52325804 and No. 52578307).

References

[1] She, W., Wang, X., Miao, C., et al. Biomimetic superhydrophobic surface of concrete: Topographic and chemical modification assembly by direct spray. *Construction and Building Materials*, **2018**, 181: 347–357. https://doi.org/10.1016/j.conbuildmat.2018.06.063.

[2] Ahmad, S. Reinforcement corrosion in concrete structures, its monitoring and service life prediction––a review. *Cement and Concrete Composites*, **2003**, 25(4/5): 459–471. https://doi.org/10.1016/S0958-9465(02)00086-0.

[3] Basheer, L., Kropp, J., Cleland, D. J. Assessment of the durability of concrete from its permeation properties: A review. *Construction and Building Materials*, **2001**, 15(2/3): 93–103. https://doi.org/10.1016/S0950-0618(00)00058-1.

[4] Bertolini, L., Elsener, B., Pedeferri, P., Redaelli, E., Polder, R. B. Corrosion of steel in concrete: prevention, diagnosis, repair. New York: John Wiley & Sons, **2013**.

[5] Basheer, P. A. M., Chidiact, S. E., Long, A. E. Predictive models for deterioration of concrete structures. *Construction and Building Materials*, **1996**, 10(1): 27–37. https://doi.org/10.1016/0950-0618(95)00092-5.

[6] Park, S. S., Kim, Y. Y., Lee, B. J., et al. Evaluation of concrete durability performance with sodium silicate impregnants. *Advances in Materials Science and Engineering*, **2014**, 2014: 945297. https://doi.org/10.1155/2014/945297.

[7] Jia, L., Shi, C., Pan, X., et al. Effects of inorganic surface treatment on water permeability of cement-based materials. *Cement and Concrete Composites*, **2016**, 67: 85–92. https://doi.org/10.1016/j.cemconcomp.2016.01.002.

[8] Jiang, L., Ma, Z., Gu, Z., et al. Impregnate carbonation: CO_2-guided *in situ* growth of robust superhydrophobic structures on concrete surfaces. *Advanced Materials*, **2024**, 36(40): 2405492. https://doi.org/10.1002/adma.202405492.

[9] Gonçalves, T., Silva, R. V., de Brito, J., et al. Mechanical and durability performance of mortars with fine recycled concrete aggregates and reactive magnesium oxide as partial cement replacement. *Cement and Concrete Composites*, **2020**, 105: 103420. https://doi.org/10.1016/j.cemconcomp.2019.103420.

[10] Liu, Y., Wang, B., Fan, Y., et al. Effects of reactive MgO on durability and microstructure of cement-based materials: Considering carbonation and pH value. *Construction and Building Materials*, **2024**, 426: 136216. https://doi.org/10.1016/j.conbuildmat.2024.136216.

[11] Dávila-Pompermayer, R., Lopez-Yepez, L. G., Valdez-Tamez, P., et al. Lechugilla natural fiber as internal curing agent in self compacting concrete (SCC): Mechanical properties, shrinkage and durability. *Cement and Concrete Composites*, **2020**, 112: 103686. https://doi.org/10.1016/j.cemconcomp.2020.103686.

[12] Alaskar, A., Alshannag, M., Higazey, M. Mechanical properties and durability of high-performance concrete internally cured using lightweight aggregates. *Construction and Building Materials*, **2021**, 288: 122998. https://doi.org/10.1016/j.conbuildmat.2021.122998.

[13] Luo, S., Wei, J., Xu, W., et al. Design, preparation, and performance of a novel organic–inorganic composite coating with high adhesion and protection for concrete. *Composites Part B: Engineering*, **2022**, 234: 109695. https://doi.org/10.1016/j.compositesb.2022.109695.

[14] Bader, T., Lackner, R. Acrylic surface treatment applied to architectural High-Performance Concrete (HPC): Identification of potential pitfalls on the way to long-lasting protection. *Construction and Building Materials*, **2020**, 237: 117415. https://doi.org/10.1016/j.conbuildmat.2019.117415.

[15] Almusallam, A. A., Khan, F. M., Dulaijan, S. U., et al. Effectiveness of surface coatings in improving concrete durability. *Cement and*

Concrete Composites, **2003**, 25(4/5): 473–481. https://doi.org/10.1016/S0958-9465(02)00087-2.

[16] Wang, H., Feng, P., Geng, Z., Liu, Q. Deterioration of organic coatings on concrete under artificial aging. In: 4th International RILEM Conference on Microstructure Related Durability of Cementitious Composites, The Hague, The Netherlands, 28–30 April, **2024**, **2021**.

[17] Wang, H., Feng, P., Lv, Y., et al. A comparative study on UV degradation of organic coatings for concrete: Structure, adhesion, and protection performance. *Progress in Organic Coatings*, **2020**, 149: 105892. https://doi.org/10.1016/j.porgcoat.2020.105892.

[18] Pan, X., Shi, Z., Shi, C., et al. A review on concrete surface treatment Part I: Types and mechanisms. *Construction and Building Materials*, **2017**, 132: 578–590. https://doi.org/10.1016/j.conbuildmat.2016.12.025.

[19] Wu, Y., Dong, L., Shu, X., et al. A review on recent advances in the fabrication and evaluation of superhydrophobic concrete. *Composites Part B: Engineering*, **2022**, 237: 109867. https://doi.org/10.1016/j.compositesb.2022.109867.

[20] Courard, L., Zhao, Z., Michel, F. Influence of hydrophobic product nature and concentration on carbonation resistance of cultural heritage concrete buildings. *Cement and Concrete Composites*, **2021**, 115: 103860. https://doi.org/10.1016/j.cemconcomp.2020.103860.

[21] Liu, H., Wang, F., Lei, S., et al. Large-area fabrication of colorful superhydrophobic coatings with high solar reflectivity. *Construction and Building Materials*, **2021**, 304: 124602. https://doi.org/10.1016/j.conbuildmat.2021.124602.

[22] Chen, H., Guo, Z., Hou, P., et al. The influence of surface treatment on the transport properties of hardened calcium sulfoaluminate cement-based materials. *Cement and Concrete Composites*, **2020**, 114: 103784. https://doi.org/10.1016/j.cemconcomp.2020.103784.

[23] Hu, X., Xiao, J., Zhang, Z., et al. Effects of CCCW on properties of cement-based materials: A review. *Journal of Building Engineering*, **2022**, 50: 104184. https://doi.org/10.1016/j.jobe.2022.104184.

[24] Li, G., Huang, X., Lin, J., et al. Activated chemicals of cementitious capillary crystalline waterproofing materials and their self-healing behaviour. *Construction and Building Materials*, **2019**, 200: 36–45. https://doi.org/10.1016/j.conbuildmat.2018.12.093.

[25] Zhan, P. M., He, Z. H. Application of shrinkage reducing admixture in concrete: A review. *Construction and Building Materials*, **2019**, 201: 676–690. https://doi.org/10.1016/j.conbuildmat.2018.12.209.

[26] Chee Ban, C., Sern, L. J., Jasme, N. The mechanical strength and drying shrinkage behavior of high performance concrete with blended mineral admixture. *Jurnal Teknologi*, **2019**, 81(4). https://doi.org/10.11113/jt.v81.13209.

[27] Huang, K., Shi, X., Zollinger, D., et al. Use of MgO expansion agent to compensate concrete shrinkage in jointed reinforced concrete pavement under high-altitude environmental conditions. *Construction and Building Materials*, **2019**, 202: 528–536. https://doi.org/10.1016/j.conbuildmat.2019.01.041.

[28] Humad, A. M., Kothari, A., Provis, J. L., et al. The effect of blast furnace slag/fly ash ratio on setting, strength, and shrinkage of alkali-activated pastes and concretes. *Frontiers in Materials*, **2019**, 6: 9. https://doi.org/10.3389/fmats.2019.00009.

[29] Tian, Y., Guo, W., Wang, W., et al. Influence of organic corrosion inhibitors on steel corrosion in concrete under the coupled action of freeze–thaw cycles and chloride attack. *Construction and Building Materials*, **2023**, 368: 130385. https://doi.org/10.1016/j.conbuildmat.2023.130385.

[30] Shehnazdeep, Pradhan, B. A study on effectiveness of inorganic and organic corrosion inhibitors on rebar corrosion in concrete: A review. *Materials Today: Proceedings*, **2022**, 65: 1360–1366. https://doi.org/10.1016/j.matpr.2022.04.296.

[31] Zhang, M. H., Islam, J. Use of nano-silica to reduce setting time and increase early strength of concretes with high volumes of fly ash or slag. *Construction and Building Materials*, **2012**, 29: 573–580. https://doi.org/10.1016/j.conbuildmat.2011.11.013.

[32] Zhang, H., Mu, S., Cai, J., et al. The impact of carboxylic acid type hydrophobic agent on compressive strength of cementitious materials. *Construction and Building Materials*, **2021**, 291: 123315. https://doi.org/10.1016/j.conbuildmat.2021.123315.

[33] Wang, K., Gou, X., Peng, L., et al. *In situ* sustained-release microcapsules to improve the impermeability of cement mortars: Preparation and characterization. *Journal of Materials in Civil Engineering*, **2023**, 35(6): 04023120. https://doi.org/10.1061/jmcee7.mteng-14551.

[34] Dong, L., Zhang, Y., Guo, Y., et al. Effects of controlled release silica nanocapsules containing sucrose on the heat release of cement hydration. *Colloids and Surfaces A: Physicochemical and Engineering Aspects*, **2023**, 670: 131593. https://doi.org/10.1016/j.colsurfa.2023.131593.

[35] Liao, Q., Zhao, X. D., Wu, W. W., et al. A review on the mechanical performance and durability of fiber reinforced lightweight concrete. *Journal of Building Engineering*, **2024**, 88: 109121. https://doi.org/10.1016/j.jobe.2024.109121.

[36] Uhrich, K. E., Cannizzaro, S. M., Langer, R. S., et al. Polymeric systems for controlled drug release. *Chemical Reviews*, **1999**, 99(11): 3181–3198. https://doi.org/10.1021/cr940351u.

[37] Kamat, A., Schlangen, E., Lubelli, B. Encapsulated crystallisation inhibitor as a long-term solution to mitigate salt damage in hydraulic mortars. *Cement and Concrete Composites*, **2024**, 152: 105682. https://doi.org/10.1016/j.cemconcomp.2024.105682.

[38] Kamat, A., Palin, D., Lubelli, B., et al. Capsule controlled release of crystallisation inhibitors in mortars. *Materials & Design*, **2024**, 244: 113156. https://doi.org/10.1016/j.matdes.2024.113156.

[39] Li, K., Zheng, H., Lu, J. X., et al. Role of encapsulated corrosion inhibitor on the anti-corrosion performance of reinforcing steel in lightweight concrete. *Cement and Concrete Composites*, **2024**, 146: 105388. https://doi.org/10.1016/j.cemconcomp.2023.105388.

[40] Wang, C., Lu, Y., Dai, Y., et al. *In-situ* 4D CT analysis of microcrack evolution in carbonated fiber-reinforced recycled aggregate concrete. *Cement and Concrete Composites*, **2025**, 163: 106161. https://doi.org/10.1016/j.cemconcomp.2025.106161.

[41] Wang, C., Yuan, J., Zhang, Y., Wu, H., Ma, Z. Advanced in-situ 4D CT reconstruction for exploring fiber distribution effects on the mechanical behaviors and interface optimization of carbonated high-toughness recycled aggregate concrete. *Construction and Building Materials*, **2025**, 473: 140941. https://doi.org/10.1016/j.conbuildmat.2025.140941.

[42] McBride, S. P., Shukla, A., Bose, A. Processing and characterization of a lightweight concrete using cenospheres. *Journal of Materials Science*, **2002**, 37(19): 4217–4225. https://doi.org/10.1023/A:1020056407402.

[43] Montgomery, D., Diamond, S. The influence of fly ash cenospheres on the details of cracking in flyash-bearing cement pastes. *Cement and Concrete Research*, **1984**, 14(6): 767–775. https://doi.org/10.1016/0008-8846(84)90001-2.

[44] Hanif, A., Lu, Z., Li, Z. Utilization of fly ash cenosphere as lightweight filler in cement-based composites–A review. *Construction and Building Materials*, **2017**, 144: 373–384. https://doi.org/10.1016/j.conbuildmat.2017.03.188.

[45] Shi, J., Liu, Y., Wang, E., et al. Physico-mechanical, thermal properties and durability of foamed geopolymer concrete containing

cenospheres. *Construction and Building Materials*, **2022**, 325: 126841. https://doi.org/10.1016/j.conbuildmat.2022.126841.
[46] Rajesh, K. N., Teena, J., Raju, P. M. A review on performance of cenosphere utilization in concrete. *Materials Today: Proceedings*, **2022**, 62: 5567–5570. https://doi.org/10.1016/j.matpr.2022.04.560.
[47] Liu, F., Wang, J., Qian, X., et al. Internal curing of high performance concrete using cenospheres. *Cement and Concrete Research*, **2017**, 95: 39–46. https://doi.org/10.1016/j.cemconres.2017.02.023.
[48] Sarkar, A., Rano, R., Mishra, K. K., et al. Characterization of cenospheres collected from ash-pond of a super thermal power plant. *Energy Sources, Part A: Recovery, Utilization, and Environmental Effects*, **2007**, 30(3): 271–283. https://doi.org/10.1080/00908310600713883.
[49] European Committee for Standardization. Methods of testing cement-Part 1: Determination of strength, EN 196-1: 2005, **2005**.
[50] European Committee for Standardization. Methods of testing cement-Part 3: determination of setting times and soundness. EN 196-3: 2005, **2005**.
[51] ASTM International. Standard Test Method for Flow of Hydraulic Cement Mortar. ASTM C1437-20, **2020**.
[52] ASTM International. Standard Test Method for Rate of Water Absorption of Masonry Mortars. ASTM C1403-15, **2015**.
[53] Noushini, A., Nguyen, Q. D., Castel, A. Assessing alkali-activated concrete performance in chloride environments using NT Build 492. *Materials and Structures*, **2021**, 54(2): 57. https://doi.org/10.1617/s11527-021-01652-7.
[54] Szewczenko, W., Kotsay, G. Influence of Water Glass Introduction Methods on Selected Properties of Portland Cement. *Materials*, **2021**, 14(12): 3257. https://www.mdpi.com/1996-1944/14/12/3257.
[55] Danish, A., Ali Mosaberpanah, M. Influence of cenospheres and fly ash on the mechanical and durability properties of high-performance cement mortar under different curing regimes. *Construction and Building Materials*, **2021**, 279: 122458. https://doi.org/10.1016/j.conbuildmat.2021.122458.
[56] Qi, Y., Li, S., Li, Z., et al. Hydration effect of sodium silicate on cement slurry doped with xanthan. *Construction and Building Materials*, **2019**, 223: 976–985. https://doi.org/10.1016/j.conbuildmat.2019.07.327.
[57] Guo, S., Zhang, Y., Wang, K., et al. Delaying the hydration of Portland cement by sodium silicate: Setting time and retarding mechanism. *Construction and Building Materials*, **2019**, 205: 543–548. https://doi.org/10.1016/j.conbuildmat.2019.02.041.
[58] Matinfar, M., Nychka, J. A. A review of sodium silicate solutions: Structure, gelation, and syneresis. *Advances in Colloid and Interface Science*, **2023**, 322: 103036. https://doi.org/10.1016/j.cis.2023.103036.
[59] Wang, X., Sun, P., Han, N., et al. Experimental study on mechanical properties and porosity of organic microcapsules based self-healing cementitious composite. *Materials*, **2017**, 10(1): 20. https://doi.org/10.3390/ma10010020.
[60] Henkensiefken, R., Castro, J., Bentz, D., et al. Water absorption in internally cured mortar made with water-filled lightweight aggregate. *Cement and Concrete Research*, **2009**, 39(10): 883–892. https://doi.org/10.1016/j.cemconres.2009.06.009.
[61] Wang, X., Xu, J., Guo, M. Hydration behavior and chloride ingress in cement mortar incorporating a novel core@shell admixture. *Cement and Concrete Composites*, **2022**, 128: 104461. https://doi.org/10.1016/j.cemconcomp.2022.104461.
[62] Wang, B., Yao, W., Stephan, D. Preparation of calcium silicate hydrate seeds by means of mechanochemical method and its effect on the early hydration of cement. *Advances in Mechanical Engineering*, **2019**, 11(4): 1687814019840586. https://doi.org/10.1177/1687814019840586.
[63] Chen, B., Zhang, Y., Chen, Q., et al., Effect of Mineral Composition and w/c Ratios to the Growth of AFt during Cement Hydration by In-Situ Powder X-ray Diffraction Analysis. *Materials*, **2020**, 13(21): 4963. https://www.mdpi.com/1996-1944/13/21/4963.
[64] Zhang, Y., Sun, C., Zhang, P., et al. Chloride absorption capacity of calcium silicate hydrate (C-S-H) and its effect on steel corrosion in simulated concrete pore solution. *Journal of Sustainable Cement-Based Materials*, **2023**, 12(12): 1548–1563. https://doi.org/10.1080/21650373.2023.2243477.

Xiangyu Zhang is a PhD candidate in Civil Engineering at the Faculty of Science and Engineering, University of Nottingham Ningbo China. He received his M.Eng. in Civil Engineering Materials from Shenzhen University in June 2024. His current research focuses on self-healing engineered cementitious composites (ECC), functional aggregates for controlled release, and durability enhancement under chloride exposure.

Leyang Lv is an Assistant Professor at Shenzhen University. He holds a PhD in Civil Engineering from the Faculty of Civil Engineering and Geosciences at Delft University of Technology in the Netherlands (ranked 2nd in the QS World University Rankings by subject). He previously worked as a building materials R&D engineer at the Asia-Pacific R&D Center of Saint-Gobain Group (a Fortune 500 company and the world's largest building materials manufacturer). After that, he joined the College of Civil and Transportation Engineering at Shenzhen University.

His current research focuses on self-healing concrete and low-carbon, high-performance cementitious materials. His research aspirations in the long term are to develop intelligent and low-carbon construction materials for the next generation of civil engineering. He was awarded the title of High-Level Overseas Talent by the Shenzhen Municipal Government. He has been granted one project from the National Natural Science Foundation of China and two research projects from Guangdong Province. He has published more than 20 SCI papers as the first or corresponding author in peer-reviewed journals such as *Cement and Concrete Research*, *Cement and Concrete Composites*, and *Construction and Building Materials* (including 15 papers in JCR Q1 journals), with a total citation count of over 600 and a Google Scholar h-index of 11.

He serves as a Young Editorial Board Member for *Intelligent Transportation Infrastructure* (ITI), Guest Editor for the international journals *Structural Concrete* and *Buildings*, and Review Editor for *Frontiers in Materials*. He is also a reviewer for various domestic and international academic journals, including *Corrosion Science*, *Construction and Building Materials*, *Journal of Structural Concrete*, and *Materials Reports*, and was recognized as an Outstanding Reviewer by *Materials Reports* in 2023. He is a member of the International Union of Laboratories and Experts in Construction Materials, Systems, and Structures (RILEM) and the Asian Concrete Federation (ACF).